Electronic Supplementary Material (ESI) for Physical Chemistry Chemical Physics.

Supporting Information: High Resolution Triple Resonance Micro Magic Angle Spinning NMR Spectroscopy of Nanoliter Sample Volumes

J. Ole Brauckmann[a,b], J.W.G. (Hans) Janssen[a], and Arno P.M. Kentgens[a,*]

[a]Institute of Molecules and Materials, Radboud University, 6500 GL Nijmegen
[b]TI-COAST, Science Park 904, 1098 XH Amsterdam
[*]Corresponding author: Tel: +31 24 36 52078; E-mail: a.kentgens@nmr.ru.nl

January 11, 2016

The microMAS probe

The microMAS probehead used in this work is designed following the same principles described as "piggy-backed" in earlier work. A hand wound solenoid microcoil is integrated into a layered vespel construction mounted on a modified 1.6 mm Varian MAS pencil stator. The rf-coil is made from an isolated copper wire with a diameter of 100 μm (115 μm with coating). The wire is wound into 10 turns. The outer and inner diameter are 605 and 375 μm respectively. Pictures of the probehead, the dimensions of the rotor and the sample-tip together with the circuitry used to connect the micro-coil are shown in figure S4. The triply-tunable rf circuit of the microcoil provides a ^{1}H channel tunable at 850 MHz with Q(^{1}H) = 130 , Q(^{13}C) = 75 at 213.7 MHz and Q(^{15}N) = 60 at 86.6 MHz resonance frequency. In figure a view onto the stator and the dimensions of the rotor and the microtip are displayed. For the X channel we measured a tuning range of 60 MHz from 163.4 to 224.1 MHz. For the Y channel the range is narrower since more capacitors are used to reach the lower frequencies. The probe can be easily changed to other frequency ranges by changing the capacitors in the tuning circuitry.

Achievable Linewidth in the Indirect Dimension

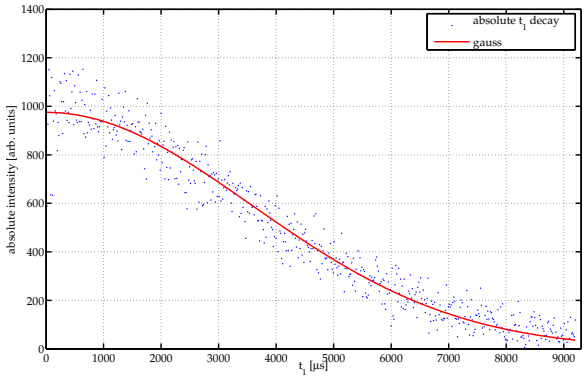

Figure S1: gaussian fit of the absolute t_1 decay recorded for the inverse detection experiment. Using equation 1 an amplitude of 975 and a σ of 5.07 ms is estimated.

To estimate the T_2^* of the inverse detection experiment, the trace at proton resonance was extracted. Since the t_1 decay is modulated by the two resonances

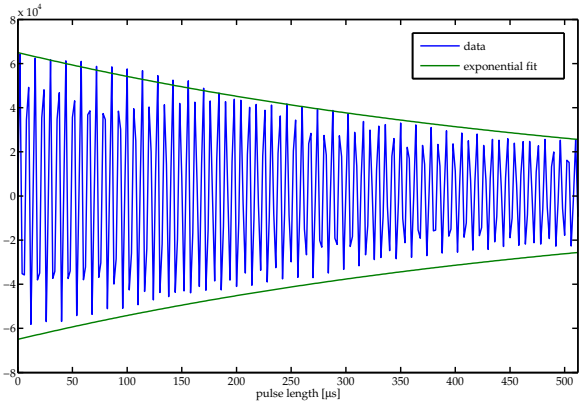

Figure S2: Nutation profile of a silicon rubber sample recorded with the microcoil. The maximum pulselength used is 512 μs. The rf-field strength was 143.6 kHz.

in the indirect dimension, the absolute signal was subjected to a gaussian model:

$$A \cdot e^{\left(-t^2/\sigma^2\right)}. \qquad (1)$$

Here A is the amplitude of the signal, t is the t_1 time and σ is the time constant of gaussian. A least square fit results in a σ of 5.07 $\pm$ 0.21ms. Since the full width at half height (FWHH) after fourier transformation of a gaussian is given by $1/\pi\sigma$ this corresponds to a maximum achievable linewidth of approximately 62.8 $\pm$ 2.5 Hz. In practice our experiment was truncated in the t_1-dimension to a maximum time of 9.2 ms. Therefore the resolution observed is limited to 110 Hz.
The fitting was performed using the curve fitting toolbox of Matlab using a gaussian model.

RF homogeneity

In S2 the signal intensity as a function of the pulselength is shown. As a measure for the homogeneity of the B_1-field often the ratio of a 810 degree pulse over a 90 degree is given. For the the silicon rubber sample this ratio is 98.1%. This indicates that the B_1 field is very homogeneous. In a nutation the linewidth in the indirect dimension indicates the inhomogeneity. Since even after 512 μs half the signal remains we estimate the inhomogeneity by an exponential fit of the decay. The green line in S2 indicates an exponential envelope with a time constant τ of 550 μs. The FWHH of a lorentzian line is given by $1/\pi\tau$ and thus the inhomogeneity is estimated to be around 580 Hz corresponding at the B_1 field of 143.6 kHz to

about 0.4%. The numbers for the homogeneity and the inhomogeneity do not add up. At shorter pulse lengths, imperfections due to phase transients during rising and falling of the voltage in the coil will affect the pulse angle and therefore the inhomogeneity measured in a full nutation is a better measurement for the characteristics of a coil. The good rf-homogeneity may explain the good performance of the micro-setup in homo- and heteronuclear decoupling experiments.

EGD DUMBO coefficients

In the table below the DUMBO coefficient used for windowed acquisition the 1D proton spectra and the proton detected HetCor experiment in the maintext are given. A proton field of $\nu_{RF}^{H} = 140$ kHz was used leading to a DUMBO period of 21.4 μs.

	EGD coeff.	
n	a_n	b_n
1	0.030119	0.153852
2	0.067404	0.166907
3	-0.000955	0.004076
4	0.067715	0.073693
5	0.059253	-0.044496
6	0.067667	0.013248

Sensitivity Enhancement by Inverse Detection

Following the derivation of Tycko, under favourable conditions it is more sensitive to record a 2D spectrum of an X-nucleus than a 1D cross-polarization spectrum. Because the enhancement that can be reached depends on the natural linewidth of the nuclei involved, sensitivity enhancements are only reached using fast magic angle spinning to narrow the proton lines and it is favourable to transfer to a low-gamma nuclei since higher enhancement factors can be reached by the ratios of the gammas.
In S3, two spectra recorded with the same number of scans are shown. The blue one is obtained by direct excitation of carbon polarization and transfer by CP to protons. The green one is obtained by direct excitation of the protons and transfer to carbons by CP and then by a second block back to protons. The spectra are scaled to the same maximum using a scaling factor of 4.16 for the blue spectrum. When the FIDs of the spectra are compared (fig S5 top), we see a similar picture: the double CP FID has much more intensity while the noise of both FIDs is comparable. The difference in intensity is caused by the CP to carbons, enhancing the polarization. By comparing the intensity of the first point of the FID, a polarization enhancement of 2.67 is estimated.

In our inverse detection experiment the sensitivity is

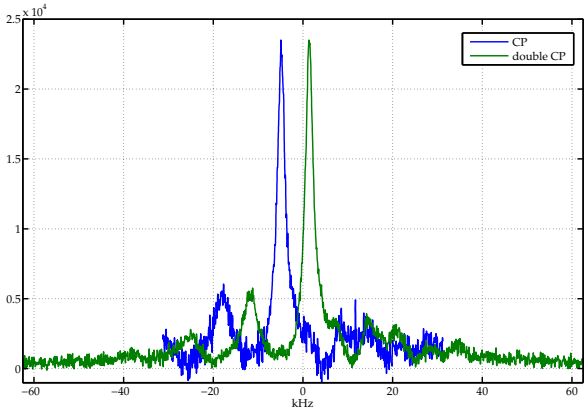

Figure S3: Comparison of the spectra obtained by double CP and CP from carbon of a 50 nL [U-^{13}C,^{15}N] glycine. The CP spectrum is scaled by a factor of 4.16 to match the intensity of the double CP spectrum.

additionally affected by the DUMBO-decoupling. In principle the total polarization should be the same, however experimentally it has been observed that especially during windowed acquisition sensitivity is lost compared to direct excitation. This has been attributed to noise introduced by switching of the hardware for the interleaved acquisition and further sensitivity might be lost by the rf-inhomogeneity throughout the sample. For DUMBO decoupling to be efficient the rf-fields have to match a 6π-modulation, however towards the end of the rf-coil, the B_1 field will decrease and probably in these regions DUMBO decoupling will be less efficient.

To take the three factors contributing to the sensitivity of the experiment into account: CP, inverse detection and DUMBO decoupling, we recorded two HetCor spectra with the DUMBO decoupling once in the indirect dimension and once in the direct dimension. Both experiments were acquired at 12.5 kHz spinning speeds and using the same rf-field and the DUMBO-1 coefficients in the indirect and dimension and during windowed acquisition. To quantify the enhancement by inverse detection we compared the ^{1}H-^{13}C correlation to a HetCor with polarization transfer from protons to carbon with DUMBO decoupling in the indirect dimension. We tried to keep the

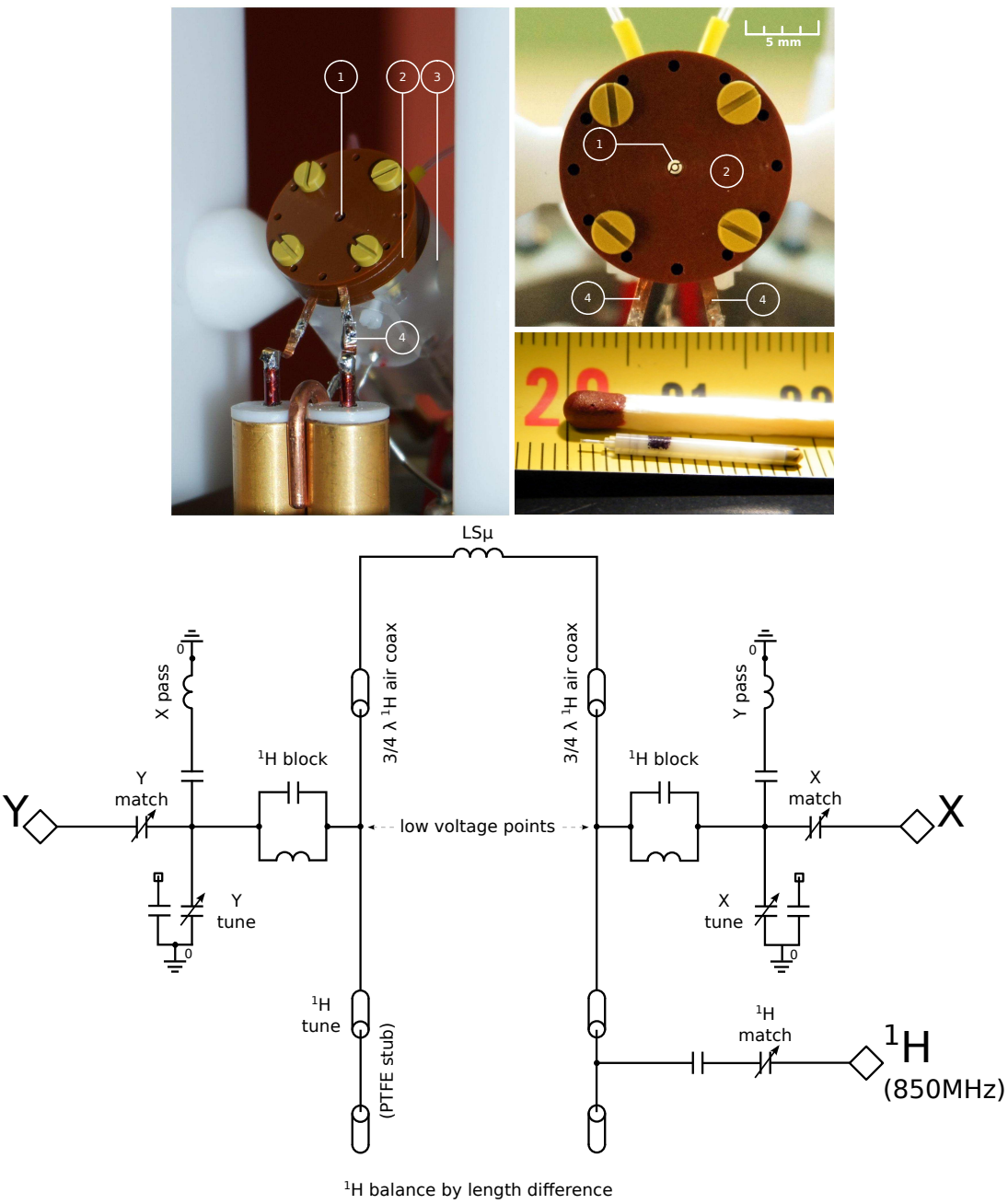

Figure S4: Top left: side view of the microMAS probehead, top left: view onto the stator and the microcoil. The numbers in the figure refer to 1) 375 μm copper microcoil (light shines through the coil), 2) the vespel construction to hold the microcoil, 3) the 1.6 mm pencil stator and 4) the contacts to the microcoil. Below a 1.6 mm rotor with a filled microtip mounted onto the rotor is shown. The rotor is placed on a metric ruler with subdivisions in millimetres together with a match as well known size reference. In the bottom of the figure the circuitry to connect the microcoil is shown.

acquisition parameters as similar as possible. However the spectral width in the proton dimension is different since the decoupling in the regular HetCor is windowless.

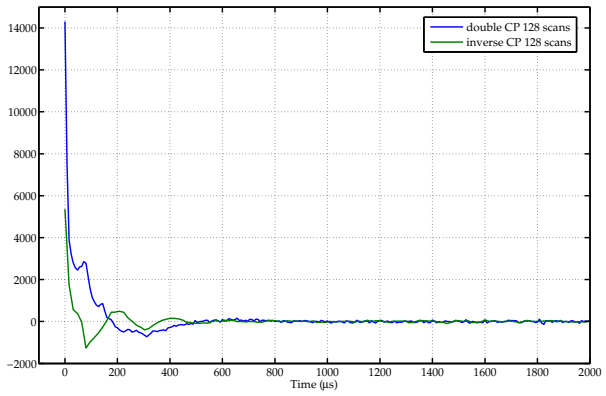

Figure S5: Top: comparison of the FIDs obtained by inverse CP from ^{13}C to ^{1}H and double CP to carbon and back of 50 nL [U-^{13}C,^{15}N] glycine with the same amount of scans.

The two HetCor spectra of uniformely labeled

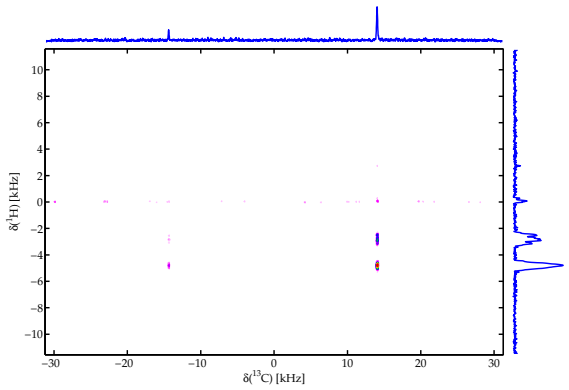

Figure S6: HetCor obtained with carbon detection using DUMBO decoupling in the indirect dimension of a 50 nL [U-^{13}C,^{15}N] glycine sample. Acquisition parameters: sw=62.5 kHz, sw1 = 23.15 kHz, ni=200, nt=4 and ACQtime = 2h13min.

glycine are shown in S6 and S7. Both spectra show in the projections the carbon and the proton spectra of glycine. We note that the proton resolution of the carbon detected HetCor is not as good as in the windowed acquisition spectra. Both spectra also show t_1-noise along the proton transmitter offset, therefore the offset should be set outside the spectral regions of interest. From the projections it is already visible that the signal to noise in the inverse detection HetCor is better.

In S8 the carbon and the proton traces in the HetCor spectra are compared. The spectra are scaled to

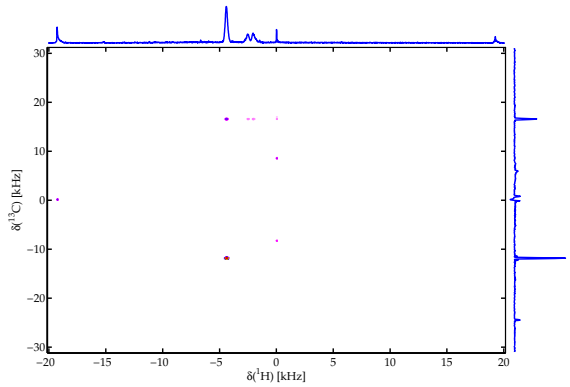

Figure S7: HetCor obtained of 50 nL [U-^{13}C,^{15}N] glycine by inverse detection using wDUMBO acquisition. Acquisition parameters: sw=40.322 sw1=62.5 kHz, ni=200, nt=4 and ACQtime=2h13min.

the same maximum. For the carbon spectra the trace along the amide resonance is shown. For the proton spectra the trace along highest intensity carbon resonance is shown. The signal to noise in the carbon trace is about a factor 5 better (128 vs 25) in an equal amount of time. For the proton traces a similar ratio is observed.

This comparison clearly shows that the inverse detection HetCor experiment is more sensitive than the carbon detected analogue.

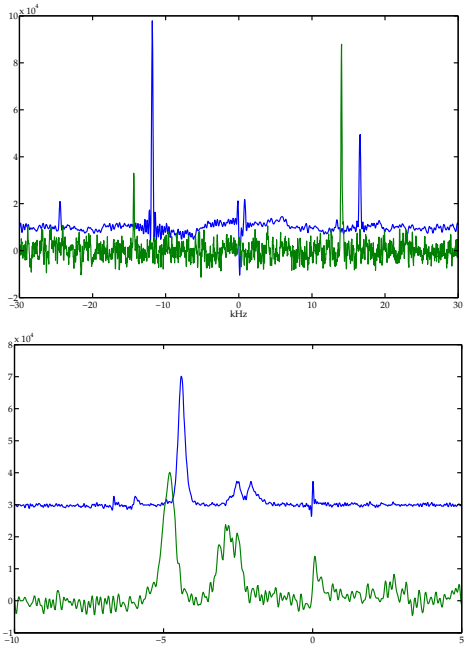

Figure S8: Comparison of the proton and the carbon traces of the carbon detected HetCor and the inverse detection HetCor using windowed DUMBO acquisition. The top of the figure compares the carbon traces, the bottom of the figure compares the proton traces.